Car collision avoidance with velocity obstacle approach

Evaluation of the reliability and performace of the collision avoidance maneuver

Maicol Laurenza, Gianluca Pepe, Dario Antonelli, Antonio Carcaterra
Mechanical and Aerospace Engineering Department
University of Rome "La Sapienza"
Rome, Italy
maicol.laurenza@uniroma1.it

***Abstract*— The obstacle avoidance maneuver is required for an autonomous vehicle. It is essential to define the system's performance by evaluating the minimum reaction times of the vehicle and analyzing the probability of success of the avoiding operation. This paper presents a collision avoidance algorithm based on the velocity obstacle approach that guarantees collision-free maneuvers. The vehicle is controlled by an optimal feedback control named FLOP, designed to produce the best performance in terms of safety and minimum kinetic collision energy. Dimensionless accident evaluation parameters are proposed to compare different crash scenarios.**

Keywords*— *Velocity obstacle; collision avoidance; optimal feedback control;

I. INTRODUCTION

The autonomous vehicle is one of the most challenging research topics that through the years has acquired such an interest due to the development of technology aiming at increasing the vehicle automation. The progressive use of increasingly cutting-edge technological solutions arises from the need to improve both transport efficiency and safety.

Recently, the introduction of autonomous driving vehicles and driver assistance systems has been strongly questioned as there is no clear regulation on the actual assessment of the safety level of such systems. A particular interest is addressed to all those systems that take the complete control of the vehicle, due to an approaching danger. As we can expect, there's no guarantee that the action taken by the system is able to avoid the accident. So, while technology can help in dangerous situations by overcoming the human limits, i.e. Reaction Time (RT), on the other hand testing and comparing the intelligent system in different scenarios and evaluate the reliability of an assisted or autonomous driving system is necessary [1-4].

The RT, in a critical situation, determines the success of the evading maneuver, as it represents the time in which the person or the artificial intelligence reacts to the external stimulus. The factors that influence the time of human reaction are related to the age of the driver, the environmental disturbances coming from both outside and inside or electronic devices such as cell phones.

This paper focuses on the analysis of critical obstacle avoidance problems in which the RT necessary to perform a safe maneuver doesn't reach the human capabilities. To achieve this task, the authors propose a robust control system suited for any vehicle as a first step to an ongoing research project of the Mechatronic and Vehicle Dynamic Lab of Sapienza [5-7]. The method is called Feedback Local Optimality Principle (FLOP) and belongs to the class of variational controls. It can take into account the nonlinearities of the dynamic model, allowing an improved performance in extreme tasks. Moreover, it allows the use of any differentiable cost function well suited for the desired maneuver. In addition, the authors propose indexes that can define the safety of a control system in different scenarios later analyzed, allowing an objective comparison.

II. OBSTACLE AVOIDANCE CONTROL MANEUVER

The self-driving vehicle usually has different levels of automation organized according to priority procedures decided *a priori*. In this work we focus on the high-level driving management architecture in which the vehicle constantly follows a set trajectory and the obstacle avoidance system intervenes when an obstacle is detected on the route. The overall architecture is represented in Fig. 1 in which the control, called FLOP, manages the steering, brake or acceleration actuators $\boldsymbol{u}$ of a vehicle to track an imposed target $\boldsymbol{x}_t$, by minimizing a given objective function $E\ (\boldsymbol{x}_t)$. The decision logic analyses the input of the road and the proprioceptive sensors $\boldsymbol{x}_{est}$ to decide when to intervene and switch the control from the simple tracking of the trajectory to the obstacle avoidance maneuver. The control strategy does not include predictive control techniques but is based on purely feedback control. This choice is due to the fact that prediction systems often require high computing performance and need time to establish an optimal control

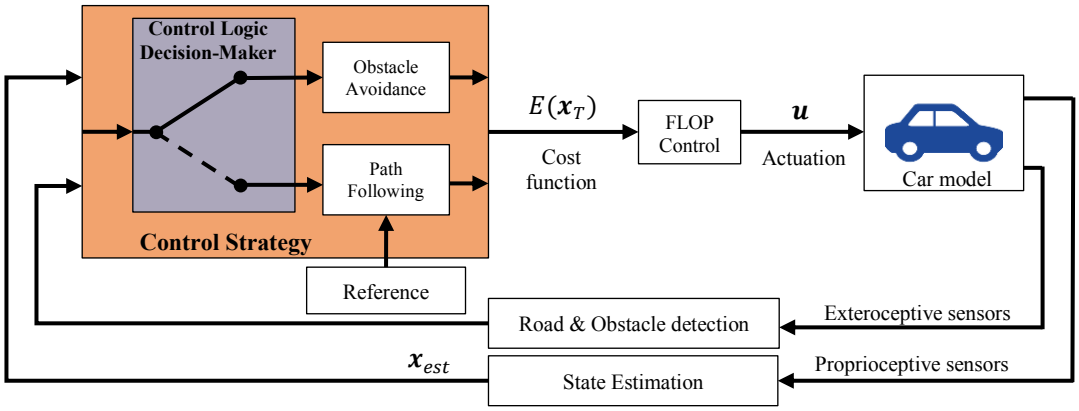

Fig. 1. The estimated state enters the control logic with road info, obstacle detections info and reference trajectory. The Decision-Maker chooses between path following or obstacle avoidance logic. The target is then fed to the FLOP control through a custom cost function, that produces the control for the vehicle.

solution. However, the control architecture has the advantage of making a forecast of the future thanks to analysis of the instantaneous speed field, able to predict the evolution of an obstacle and then choose the best maneuver.

In this work it is studied how the FLOP can control the vehicle during incipient accident, in which the estimated time of crash is approximately 1-2 seconds. The following paragraphs illustrate the autonomous driving simulator. First of all, the dynamic model of the vehicle is described, then the operation of the FLOP control is explained and finally the operation of the obstacle avoidance strategy in the speed field is described in detail. In conclusion, the performance of the new architecture is analyzed by analyzing different accident scenarios and defining an index for estimating the quality of global control.

III. VEHICLE MODEL

The dynamic system chosen for the analysis of the obstacle avoidance maneuver is the classic bike model (Fig. 2) with 3 degrees of freedom, longitudinal, lateral and yaw motion and three degrees of control, the front steering wheel and the rear and front torques. The bike model depicted in Fig. 2 has the longitudinal and lateral velocities in the body reference u,v, respectively, and the yaw angle rate ω. The rotation speed of both front and rear wheels is ω_f and ω_r, respectively. The generalized speed $\boldsymbol{\nu}$ is expressed in the body reference frame as $\boldsymbol{\nu} = [u, v, \omega, \omega_f, \omega_r]^T$; the position of the center of gravity in the earth fixed frame, is expressed by X and Y that together with the vehicle orientation ψ produces $\boldsymbol{\eta} = [X, Y, \psi]^T$. The control variables are the front wheel steering angle δ and the torque on both the rear and front wheel, named C_r and C_f, respectively. The equations of motion have the form:

$$\begin{aligned} \boldsymbol{M}\dot{\boldsymbol{\nu}} + \boldsymbol{C}(\boldsymbol{\nu})\boldsymbol{\nu} &= \boldsymbol{\tau} \\ \dot{\boldsymbol{\eta}} &= \boldsymbol{J}(\psi)\boldsymbol{\nu} \end{aligned} \tag{1}$$

where

$$\boldsymbol{M} = diag[m, m, I_z, I_w, I_w]$$

$$\boldsymbol{C}(\boldsymbol{\nu}) = \begin{bmatrix} 0 & m\omega & 0 & 0 & 0 \\ -m\omega & 0 & 0 & 0 & 0 \\ 0 & 0 & 0 & 0 & 0 \\ 0 & 0 & 0 & 0 & 0 \\ 0 & 0 & 0 & 0 & 0 \end{bmatrix}$$

$$\boldsymbol{J}(\psi) = \begin{bmatrix} \cos(\psi) & -\sin(\psi) & 0 \\ \sin(\psi) & \cos(\psi) & 0 \\ 0 & 0 & 1 \end{bmatrix}$$

$$\boldsymbol{\tau} = \begin{bmatrix} F_{long_f}\cos(\delta) - F_{lat_f}\sin(\delta) + F_{long_r} \\ F_{long_f}\sin(\delta) + F_{lat_f}\cos(\delta) + F_{lat_r} \\ F_{long_f}\sin(\delta)\, l_f + F_{lat_f}\cos(\delta)\, l_f - F_{lat_r} l_r \\ C_f + r_w F_{long_f} - C_{roll_f} \\ C_r + r_w F_{long_r} - C_{roll_r} \end{bmatrix}$$

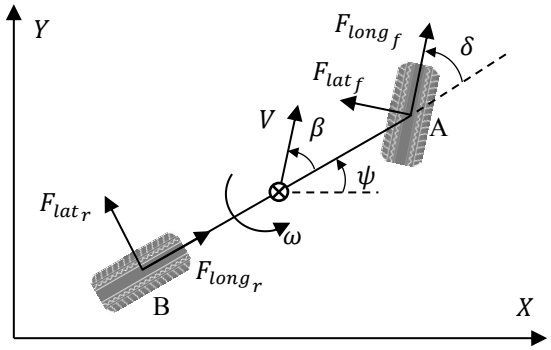

Fig. 2. Bike model

where $m, I_z, I_w, l_f, l_r, r_w, F_{long}, F_{lat}, C_{rolling}$ are the vehicle mass, the vehicle body rotational inertia, the wheel rotational inertia, the rear and front wheel distance from the center of gravity, the wheel radius, the longitudinal and lateral Pacejka forces and the rolling resistance, respectively. The contact forces are modelled by the Pacejka model. The Pacejka model uses nonlinear functions in terms of the longitudinal and lateral slip ratios σ, α , together with a linear dependence on the normal forces F_N acting on the wheels. Nowadays it is possible to measure the real time conditions of the tires grip, thanks to the development of embedded sensors such as in [8]. The rolling resistance is a quadratic function of the longitudinal speed:

$$F_{long}(F_N, \sigma, \alpha)\ ;\ F_{lat}(F_N, \sigma, \alpha)\ ;\ C_{roll}(u, F_N) \qquad (2)$$

Now arranging in a first order dynamic system with the state variable $\boldsymbol{x} = [\boldsymbol{\eta}, \boldsymbol{v}]^T$ and the control variable $\boldsymbol{u} = [\delta, C_f, C_r]^T$ we have the general form:

$$\dot{\boldsymbol{x}} = \boldsymbol{\phi}(\boldsymbol{x}) + \boldsymbol{h}(\boldsymbol{x}, \boldsymbol{u}) \qquad (3)$$

IV. A RESUME OF THE FEEDBACK CONTROL LAW FLOP

The control technique developed by the authors belongs to the class of variational controls but use a local optimality principle instead of a global one [4-6]. The problem statement is the classical one, with a performance index $\bar{J}$, integral of the cost function $E(\boldsymbol{x}, \boldsymbol{u})$ subject to the dynamic equation of the system, that is minimized (or maximized) along the time interval $[0, T]$:

$$\min \bar{J} = \int_0^T E(\boldsymbol{x}, \boldsymbol{u}) dt$$

subject to (4)

$$\dot{\boldsymbol{x}} = \boldsymbol{f}(\boldsymbol{x}(t), \boldsymbol{u}(t))$$

$$\boldsymbol{x}(0) = \boldsymbol{x_0}$$

that leads to

$$\min J = \int_0^T E(\boldsymbol{x}, \boldsymbol{u}) + \boldsymbol{\lambda}^T(\dot{\boldsymbol{x}} - \boldsymbol{f}(\boldsymbol{x}, \boldsymbol{u}))\, dt \qquad (5)$$

where $\boldsymbol{x}$ is the system state and $\boldsymbol{u}$ is the control vector. The dynamic equation of the controlled system $\dot{\boldsymbol{x}} = \boldsymbol{f}(\boldsymbol{x}, \boldsymbol{u}, t)$ with its known initial condition $\boldsymbol{x}(0) = \boldsymbol{x_0}$ represents a constraint between $\boldsymbol{x}$ and $\boldsymbol{u}$, introduced through the Lagrange multiplier $\boldsymbol{\lambda}(t)$. The solution to (4) provides both the optimal control $\boldsymbol{u}^*(t)$ and the corresponding optimal trajectory $\boldsymbol{x}^*(t)$.

The Feedback Local Optimality Principle-FLOP consists of dividing integral (5) into $N = T/\Delta\tau$ sub-integrals, where $\Delta\tau$ is the time horizon of each one. Then the minimization is applied to every integral leading to local optimality criterion:

$$J = \sum_{i=1}^{N} J_i = \sum_{i=1}^{N} \int_{LB_i}^{UB_i} \mathcal{L}(\dot{\boldsymbol{x}}, \boldsymbol{x}, \boldsymbol{u}, \boldsymbol{\lambda}) dt$$

$$\min(J_i)\ \forall\ i \qquad (6)$$

where UB_i and LB_i limits are the *upper bound* and *lower bound* for each time interval, respectively. Moreover, for each interval, the transversality conditions hold:

$$\boldsymbol{x}_{LB_i} = \boldsymbol{x}_{UB_{i-1}} \quad ; \quad \boldsymbol{\lambda}_{UB_i} = \boldsymbol{0} \qquad (7)$$

The advantage of this approach is the chance of obtaining a feedback control law without the limitation of having a quadratic cost function and a linear dynamic model. However, there are some limitations to meet. The dynamic model has to be of the type $\dot{\boldsymbol{x}} = \boldsymbol{\phi}(\boldsymbol{x}) + \boldsymbol{B}\boldsymbol{u}$, where $\boldsymbol{\phi}(\boldsymbol{x})$ is differentiable in the state space. The cost function has to be of the type $\frac{1}{2}\boldsymbol{u}^T\boldsymbol{R}\boldsymbol{u} + g(\boldsymbol{x})$, where $g(\boldsymbol{x})$ is also differentiable in the state space. On the other hand, this allows to use every function best suited for the task assigned to the model, especially for the obstacle avoidance as it can be chosen a function that is limited in the state space instead of a quadratic one. The last disadvantage is the fact that the found solution is a sub-optimal one with respect to the classical approach and is sensitive to the parameter $\Delta\tau$.

So, the problem statement including the generalization of the cost function by $g(\boldsymbol{x})$, and the formulation for the dynamics, is:

$$min\, J = \int_0^T \frac{1}{2}\boldsymbol{u}^T\boldsymbol{R}\boldsymbol{u} + g(\boldsymbol{x}) + \boldsymbol{\lambda}^T\left(\dot{\boldsymbol{x}} - (\boldsymbol{\phi}(\boldsymbol{x}) + \boldsymbol{B}\boldsymbol{u})\right) dt \qquad (8)$$

to which is applied the Euler-Lagrange method:

$$\begin{cases} \nabla_{\boldsymbol{x}} g - \nabla_{\boldsymbol{x}}\boldsymbol{\phi}^T\boldsymbol{\lambda} - \dot{\boldsymbol{\lambda}} = \boldsymbol{0} \\ \boldsymbol{R}^T\boldsymbol{u} - \boldsymbol{B}^T\boldsymbol{\lambda} = \boldsymbol{0} \quad \forall t \in [0, T] \\ \dot{\boldsymbol{x}} = \boldsymbol{\phi}(\boldsymbol{x}) + \boldsymbol{B}\boldsymbol{u} \end{cases} \qquad (9)$$

At this point we apply the local optimality principle through finite difference technique with a time step equal to the integration step $\Delta\tau$. This leads to:

$$\dot{\boldsymbol{\lambda}} \approx \frac{\boldsymbol{\lambda}_{UB_i} - \boldsymbol{\lambda}_{LB_i}}{\Delta\tau} = -\frac{\boldsymbol{\lambda}_{LB_i}}{\Delta\tau}$$

$$\nabla_{\boldsymbol{x}} g|_{LB_i} - \nabla_{\boldsymbol{x}}\boldsymbol{\phi}^T|_{LB_i}\boldsymbol{\lambda}_{LB_i} + \frac{\boldsymbol{\lambda}_{LB_i}}{\Delta\tau} = \boldsymbol{0} \qquad (10)$$

solve for $\boldsymbol{\lambda}_{LB_i}$:

$$\boldsymbol{\lambda}_{LB_i} = \left[\nabla_{\boldsymbol{x}}\boldsymbol{\phi}^T|_{LB_i} - \frac{1}{\Delta\tau}\boldsymbol{I}\right]^{-1} \nabla_{\boldsymbol{x}} g|_{LB_i} \qquad (11)$$

This expression, substituted into the second equation of (9), leads to:

$$\boldsymbol{u}_{LB_i} = \boldsymbol{R}^{-T}\boldsymbol{B}^T\left[\nabla_{\boldsymbol{x}}\boldsymbol{\phi}^T|_{LB_i} - \frac{1}{\Delta\tau}\boldsymbol{I}\right]^{-1} \nabla_{\boldsymbol{x}} g|_{LB_i} \qquad (12)$$

V. OBSTACLE AVOIDANCE

There are several techniques that are used for identifying the obstacles [9-11] and here, for the first time, the Velocity Obstacles (VO) method is used in the automotive field. The VO technique brings the analysis to the velocity space of the vehicle, then allowing a predictive control. The speed space in which an accident is predicted is defined by two categories of obstacles: (i) the finite-sized obstacles such as vehicles, pedestrians, bicycles, etc. and (ii) the infinite length of obstacles i.e. the edges of the road.

A. *The VO area for finite-sized obstacles*

The VO area for finite-sized obstacle consists of the Minkowsky sum of the two vehicles geometric shapes [12], identifying un unsafe sub-space of relative velocities that will cause future accidents (Fig. 3).

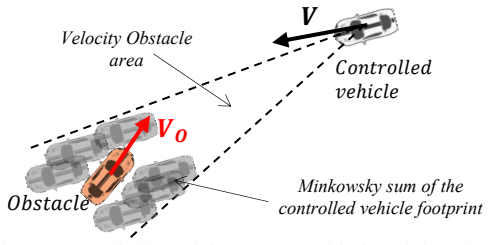

Fig. 3. Definition of the VO area with the Minkowsky sum.

Then the VO area is translated of the $\boldsymbol{V}_O$ obstacle velocity to identify the sub-space of velocities in the fixed reference frame where the velocity vector of the controlled vehicle $\boldsymbol{V}$ doesn't have to fall to avoid the accident.

B. *The VO area for the road boundary*

Since the edge of the road is an infinite object, the classic VO with the sum of Minkowsky cannot be applied. In this case, the critical speed area (VO area) is identified a priori by a parallel line to the edge of the road (Fig. 4).

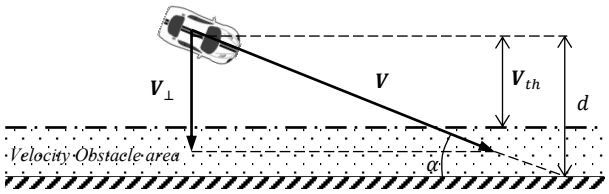

Fig. 4. The road obstacle identification in the velocity space.

The velocity threshold $\boldsymbol{V}_{th}(\boldsymbol{V}, \alpha, d)$ is a function of the dynamic behavior of the vehicle, i.e. the vehicle speed $\boldsymbol{V}$, its orientation α and the distance d from the boundary road (see figure 5). The $\boldsymbol{V}_{th}$ is found by several numerical tests and it identify the maximum orthogonal speed component ($\boldsymbol{V}_\perp$) before the roadside avoidance control is activated. The threshold is performed, so as, to control the vehicle without risking an accident. Instead, if the condition $\|\boldsymbol{V}_\perp\| < \|\boldsymbol{V}_{\text{th}}\|$ is satisfied, the vehicle is free to move.

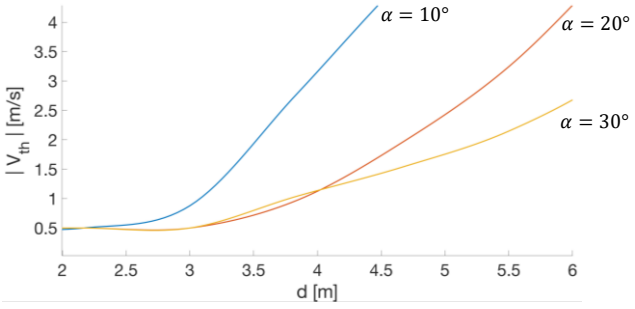

Fig. 5. The velocity thershold in fuction of the road distance d, the speed orientation α for a fixed speed $\boldsymbol{V}$.

VI. THE OBSTACLE AVOIDANCE CONTROL IN EXAMPLE SCENARIO

The Fig. 6 shows a general crash scenario in the velocity space where the velocity of the vehicle $\boldsymbol{V}$ is in the VO area (i.e. the P_A point). As we can see, the velocity space is limited by the road boundaries and the *upper-lower observation limits*. These last depend on the characteristics of the vehicle itself and are tuning parameters. The upper limit observation is in function of the acceleration capability of the vehicle and it changes proportionally varying the speed $\boldsymbol{V}$, viceversa, the lower limit is function of the brake capabilities of the vehicle. The resulting area is divided by several crash areas (red) and free ones (green). The widest no-crash area represents the target zone where the vehicle is brought in to the P_T target point. The obstacle avoidance is active until there is at least a cone red area.

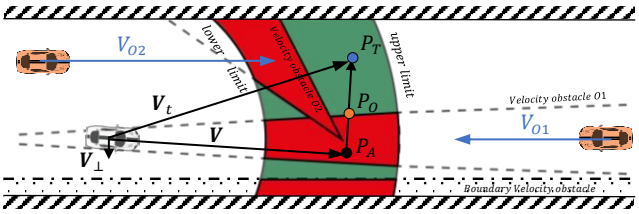

Fig. 6. Velocity space for obstacle avoidance maneuvering.

Once an obstacle avoidance maneuver is turned on, the standard cost function to follow the path trajectory [13] is abandoned and the $g(\boldsymbol{x})$ cost function defined in (8) is switched in $g_{OA}(\boldsymbol{x})$ where the target point P_T is reached in function of the yaw, the angular velocity and the lateral-longitudinal speed targets.

$$g_{OA}(\boldsymbol{x}) = g_1(\psi) + g_2(\omega) + g_3(u, v)$$

with

$$g_1(\psi) = \frac{1}{2} q_1 (\psi - \psi_T)^2 \qquad (13)$$
$$g_2(\omega) = \frac{1}{2} q_2 \omega^2$$
$$g_3(u, v) = \frac{1}{2} (\boldsymbol{V} - \boldsymbol{V}_t)^T \boldsymbol{Q}(\|\boldsymbol{V} - \boldsymbol{V}_t\|)(\boldsymbol{V} - \boldsymbol{V}_t)$$

where q_1, q_2 and the matrix $\boldsymbol{Q}$ are tuning coefficients. The g_1 function is useful to orient the yaw of the vehicle along the P_T direction, the g_2 is needed to mitigate the angular speed and finally the g_3 is to establish a smooth rate of change of speed in order to reach the desired target speed. The gradient of g_3 is plotted in Fig. 7 where, thanks to the variability of the $\boldsymbol{Q}$-gains proportionally to the norm $\|\boldsymbol{V} - \boldsymbol{V}_t\|$, the vehicle is quickly moved away from the crash area and slowly drawn into the safest zone.

I. SAFETY INDEXES

In order to assess the quality of a control logic, three indexes have been defined to analyze the quality of a maneuver: (i) the probability of a crash, (ii) the analysis of kinetic energy exchanged during the impact, and finally (iii) the minimum obstacle avoidance distance. All three

parameters are assessed according to the type of scenario and the vehicle and obstacle condition.

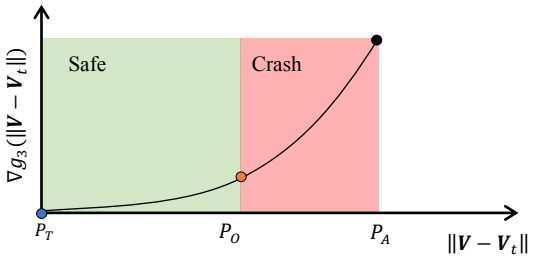

Fig. 7. Gradient of custom cost function: the shape is accustomed to let the slope be hight in the *VO* area and smooth in the safe area.

The probability of crash P is the ratio between the simulations which end with a crash, and the total number of simulations.

$$P = \frac{N_{crashes}}{N_{simulations}}\% \tag{14}$$

The probability of crash is studied in function of a dimensionless parameter χ that represent the ratio between the free maneuver time τ_m and crash time τ_c so defined:

$$\chi = \frac{\tau_m}{\tau_c} \tag{15}$$

The free maneuver time τ_m, is the ratio between the free lateral space $(L - C - C_O)$, i.e. L the carriage width, C and C_O the lateral obstructed space of the controlled and uncontrolled vehicle, over the speed of the controlled vehicle $\|\boldsymbol{V}\|$ (see Fig. 9):

$$\tau_m = \frac{L - C - C_O}{\|\boldsymbol{V}\|} \tag{16}$$

Instead the time crash τ_c gives the information about how long it takes to do an accident:

$$\tau_c = \frac{d}{\|\boldsymbol{V} - \boldsymbol{V}_O\|} \tag{17}$$

where d is the relative distance between the controlled vehicle and the obstacle.

The second quality index is related to the crash cases and analyzes the severity of the accidents through the evaluation of the kinetic energy involved K.

$$K = \frac{1}{2} m V_{\hat{n}}{}^2 \tag{18}$$

where the $V_{\hat{n}}$ is the orthogonal crash component, i.e. along $\hat{n}$, of the relative impact speed $\boldsymbol{V}_O - \boldsymbol{V}$ between the controlled vehicle and the obstacle (see Fig. 8).

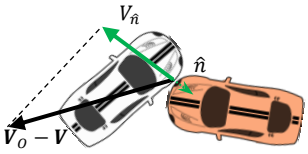

Fig. 8. Orthogonal component to the vehicle of the relative velocity of the crash.

The last index is the minimum distance d_{min} between the vehicles during the successful maneuvers. This parameter defines the degree of reliability of the maneuver, in fact, even if the crash is avoided it is useful to check how far the controlled vehicle has passed.

II. Simulations and Results

In this section, the performances of the proposed control system are investigated in the frontal, the plugging and the crossroad crash scenarios. The random simulations are built in a way that the initial velocity of the controlled vehicle is always in the *VO* area, i.e. always in crash condition. The varying parameters are equals for the different scenarios: the initial speed of both the controlled vehicle and the obstacle ($\boldsymbol{V}$ and $\boldsymbol{V}_O$), the initial yaw (ψ and ψ_O), the initial position and distance as is shown in figures 9 and 10. The crossroad scenario is tested also varying the angle γ of the of the side lane (see fig. 10). The obstacle velocity is constant through the entire simulation.

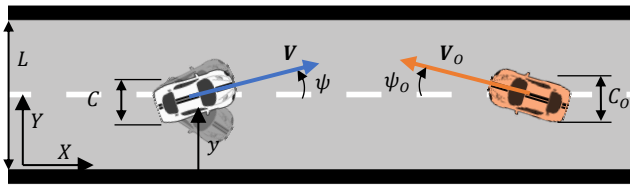

Fig. 9. Frontal crash scenario.

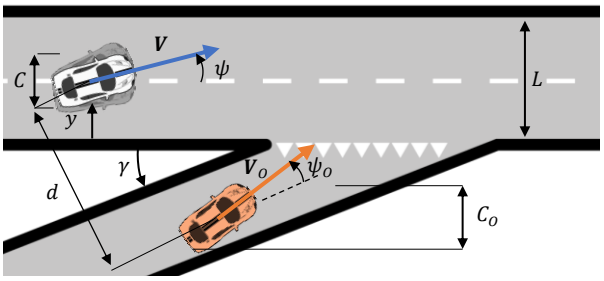

Fig. 10. Crossroad crash scenario.

The results of the simulations are expressed according to the following figures, going to investigate the probability of accident, the severity of the accidents not avoided, the minimum distance between the two vehicles of the avoidance maneuver.

From Fig. 11 it is noted that at a value of 0.27 of χ, the *Frontal* curve has a knee, after which it shows a very high positive slope. The high value means a strong separation between the safe zone and the incident zone, indicating the achievement of a physical limit of the scenario. The presence of the knee also suggests that it is not possible to avoid all

accidents, since not all the maneuvers required to avoid the vehicle belong to the configuration space reached by the same. Regarding the *Plugging* curve, it can be seen that the keen is near the *Frontal* one, showing a similar behavior between the scenarios, although the *Plugging* one has a stronger slope. Regarding the *Crossroad* curve we see a slightly different trend with respect to the previous curves, where the χ corresponding to the knee is greater and the slope is softer. This is because the obstruction of the obstacle is greater, being on the side compared to the controlled vehicle. It is therefore important to analyze the danger from the point of view of the kinetic energy involved.

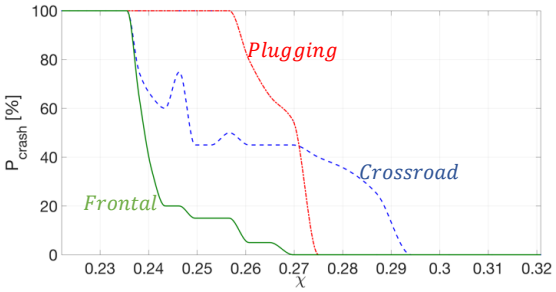

Fig. 11. Probability of crash for different crash scenarios.

The Fig. 12 shows the comparison of the mean kinetic energy between different scenarios. The evolution of kinetic energy gives us the possibility to evaluate the seriousness of the accident even in all those cases where the probability is close to 100%. In the figure 12 is shown how the frontal accident reaches higher values of kinetic energy for low χ.

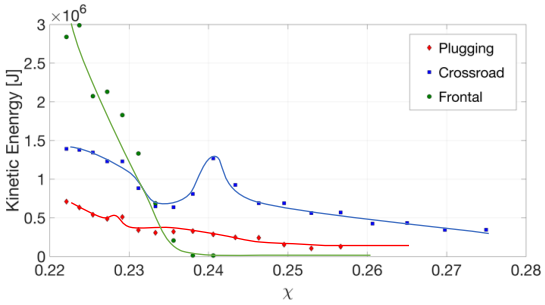

Fig. 12. Kinetic energy involved in the different scenarios.

Finally, the trend of the minimum distances between the vehicles for the avoidance maneuvers are shown. We can see in Fig. 13 that the vehicle performs safer maneuvers for higher values of χ.

I. Conclusions

The authors present a new control algorithm for avoidance of obstacles for autonomous driving vehicles. The VO based control system is used purely in feedback to increase the computational performance usually required by more elaborate controllers such as the NMPC. The performance of the controlled system is assessed by observing quality analysis indices of the avoidance maneuver. All the maneuvers are performed starting from a limit condition in which the vehicle finds itself in a potential accident condition. The FLOP control, used to drive the vehicle, makes it possible to manage nonlinear dynamic systems, thus keeping the real vehicle's characteristics unchanged. Moreover, the optimal variational control FLOP gives the possibility to use nonlinear cost functions in the state, allowing to test different shapes of useful functions for the improvement of the maneuver.

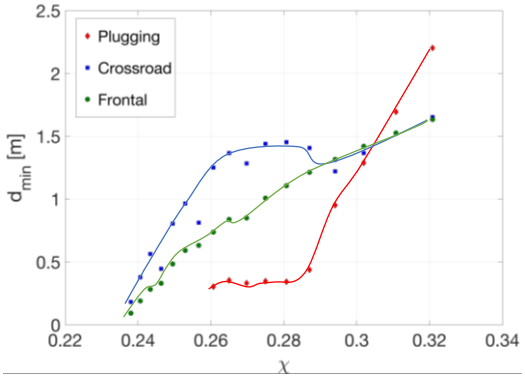

Fig. 13. Minimum distances between the vehicles for the successful maneuvers in different scenarios.

References

[1] Matija Svetina, “The reaction times of drivers aged 20 to 80 during a divided attention driving”, Traffic Injury Prevention, 17:8, 810-814, 2016.

[2] Q. Wang, B. Ayalew and T. Weiskircher, "Predictive Maneuver Planning for an Autonomous Vehicle in Public Highway Traffic", in IEEE Transactions on Intelligent Transportation Systems, vol. 20, no. 4, 1303-1315, April 2019.

[3] W. Liu and Z. Li, "Comprehensive predictive control method for automated vehicles in dynamic traffic circumstances", in IET Intelligent Transport Systems, vol. 12, no. 10, 1455-1463, 12 2018.

[4] D. Antonelli, L. Nesi, G. Pepe, A. Carcaterra, “A novel control strategy for autonomous cars”, ACC 2019, Philadelphia, USA, 2019, in press.

[5] D. Antonelli, L. Nesi, G. Pepe and A. Carcaterra, “A novel approach in Optimal trajectory identification for Autonomous driving in racetrack”, ECC 2019, Naples, Italy, 2019, in press.

[6] D. Antonelli, L. Nesi, G. Pepe, A. Carcaterra, “Mechatronic control of the car response based on VFC”, ISMA2018, Leuven, Belgium, 2018.

[7] P. Gianluca, N. Roveri, A. Carcaterra, ”Prototyping a new car semi-active suspension by variational feedback controller”, ISMA 2016, Leuven, Belgium, 2016.

[8] F. Coppo, G. Pepe, N. Roveri, A. Carcaterra, “A multisensing setup for the intelligent tire monitoring”, Sensors (Switzerland), 17 (3), art. no. 576, 2017.

[9] Febbo, H., Liu, J., Jayakumar, P., Stein, J. L., & Ersal, T., “Moving obstacle avoidance for large, high-speed autonomous ground vehicles”, Proceedings of the American Control Conference, 5568-5573, 2017.

[10] Liu, J., Jayakumar, P., Stein, J. L., & Ersal, T. (2018), “A nonlinear model predictive control formulation for obstacle avoidance in high-speed autonomous ground vehicles in unstructured environments”, Vehicle System Dynamics, 56(6), 853-882, 2018.

[11] Hu, Xuemin & Chen, Long & Tang, Bo & Cao, Dongpu & He, Haibo., “Dynamic path planning for autonomous driving on various roads with avoidance of static and moving obstacles”, Mechanical Systems and Signal Processing, 100, 482-500, 2018.

[12] Snape, J., Van Den Berg, J., Guy, S. J., & Manocha, D., “The hybrid reciprocal velocity obstacle”, IEEE Transactions on Robotics, 27(4), 696-706, 2011.

[13] Chen, Te & Chen, Long & Xu, Xing & Cai, Yingfeng & Sun, Xiaoqiang, “Simultaneous path following and lateral stability control of 4WD-4WS autonomous electric vehicles with actuator saturation”, Advances in Engineering Software, 128, 46-54, 2019.